Structure, Vol. 12, 949–959, June, 2004, ©2004 Elsevier Ltd. All rights reserved. DOI 10.1016/j.str.2004.03.026

The First Crystal Structure of the Novel Class of Fructose-1,6-Bisphosphatase Present in Thermophilic Archaea

Hiroshi Nishimasu,[1] Shinya Fushinobu,[1] Hirofumi Shoun, and Takayoshi Wakagi*
Department of Biotechnology
The University of Tokyo
1-1-1 Yayoi, Bunkyo-ku, Tokyo 113-8657
Japan

Summary

As the first structure of the novel class of fructose-1,6-bisphosphatase (FBPase) present in thermophilic archaea, we solved the crystal structure of the ST0318 gene product (St-Fbp) of *Sulfolobus tokodaii* strain 7. The St-Fbp structure comprises a homooctamer of the 422 point-group. The protein folds as a four-layer α-β-β-α sandwich with a novel topology, which is completely different from the sugar phosphatase fold. The structure contains an unhydrolyzed FBP molecule in the open-keto form, as well as four hexacoordinated magnesium ions around the 1-phosphoryl group of FBP. The arrangement of the catalytic side chains and metal ligands is consistent with the three-metal ion assisted catalysis proposed for conventional FBPases. The structure provides an insight into the structural basis of the strict substrate specificity of St-Fbp.

Introduction

Fructose-1,6-bisphosphatase (D-fructose-1,6-bisphosphate 1-phosphohydrolase, EC 3.1.3.11., hereafter called FBPase) is an essential regulatory enzyme in the gluconeogenic pathway (Shieh and Chiang, 1998). FBPase catalyzes the hydrolysis of D-fructose-1,6-bisphosphate (FBP) to D-fructose-6-phosphate (F6P) and orthophosphate (Pi). It is the reverse of the reaction of phosphofructokinase in glycolysis, and the product, F6P, is an important precursor in various biosynthetic pathways. Because the inhibition of FBPase in mammals results in a reduced level of serum glucose in the fasting state, FBPase is a target for the development of drugs for the treatment of noninsulin-dependent diabetes (DeFronzo, 1999; Wright et al., 2002).

Donahue et al. proposed a classification of eukaryal/bacterial FBPases into three groups (FBPase I–III) (Donahue et al., 2000). In most archaeal genomes, genes homologous to those FBPases (FBPase I–III) are not present; thus, archaeal FBPase genes have not been identified. Stec et al. reported that the MJ0109 gene product from *Methanococcus jannaschii* exhibits the dual activities of FBPase and inositol monophosphatase (IMPase) (Stec et al., 2000). The products of homologous genes in *Archaeoglobus fulgidus* and *Thermotoga maritima* also exhibit FBPase/IMPase dual activity. The *Pyrococcus furiosus fbpA* gene product shows a preference for FBP as the substrate, and these newly identified archaeal FBPases are classified as FBPase IV (Verhees et al., 2002). So far, the crystal structures of two class IV FBPases, MJ0109 from *M. jannaschii* (Johnson et al., 2001; Stec et al., 2000) and AF2372 from *A. fulgidus* (Stieglitz et al., 2002), have been reported. FBPases I and IV, and eukaryal/bacterial IMPases share a common sugar phosphatase fold.

Recently, Rashid et al. found a new FBPase in *Thermococcus kodakaraensis* KOD1 (Tk-Fbp), whose amino acid sequence (PH0759) is completely different from those of known FBPases (Rashid et al., 2002). Tk-Fbp exhibits strict substrate specificity to FBP, and its activity is enhanced by the Mg^{2+} ions. Tk-Fbp exhibits a slightly higher K_m value and an about 2-fold higher k_{cat} value at 95°C than those measured for the MJ0109 gene product at 85°C. The gene expression of Tk-Fbp is regulated at the transcription level. Genes homologous to that of Tk-Fbp are present in all the known complete genome sequences of thermophilic archaea, including those of *M. jannaschii* (MJ0299), *P. furiosus* (PF0613), *A. fulgidus* (AF1442), and *Sulfolobus solfataricus* (SSO0286). Rashid et al. (2002) proposed that the new FBPase family can be taken as the bona fide FBPases in archaea. Hereafter, we designate it as the FBPase V family (Verhees et al., 2003). FBPase V family is present in the genomes of all thermophilic archaea and a hyperthermophilic bacterium, *Aquifex aeolicus*, but not in nonthermophilic organisms (Rashid et al., 2002).

Sulfolobus tokodaii strain 7 is a strictly aerobic and thermoacidophilic archaeon isolated from Beppu hot spring, Kyushu, Japan, and grows optimally at pH 2–3 and 75°C–80°C on glucose as the sole carbon source (Kawarabayasi et al., 2001). *Sulfolobus* is thought to use an Entner-Doudoroff-like glycolysis pathway in which the activation via phosphorylation occurs at a later stage in the pathway: at the level of glycerate (Verhees et al., 2003). However, the organism has been shown to also use another route to metabolize glucose, which involves an ATP-dependent phosphorylation and subsequent isomerization of glucose 6-phosphate to fructose 6-phosphate (De Rosa et al., 1984). Moreover, *Sulfolobus* has been demonstrated to have a capacity to generate glucose polymers (glycogen) as storage material, suggesting the presence of gluconeogenesis pathway in this organism (Konig et al., 1982). However, detailed characteristics of its gluconeogenic enzymes are still unknown. *S. tokodaii* possesses a FBPase IV gene (ST0547), as well as a FBPase V gene (ST0318). The ST0318 gene product displays 63% amino acid identity to Tk-Fbp.

Here we report the characterization of the ST0318 gene product of *S. tokodaii* strain 7 (St-Fbp), and its crystal structure in complex with FBP and Mg^{2+} ions. The catalytic mechanism of the metal-dependent FBPase activity and the novel fold of FBPase V are also revealed.

Results and Discussion

Characterization of the Recombinant Enzyme

The ST0318 gene was cloned and expressed in *Escherichia coli*. The purified St-Fbp enzyme exhibited signifi-

*Correspondence: atwakag@mail.ecc.u-tokyo.ac.jp
[1]These authors contributed equally to this work.

Table 1. Activity of the Wild-Type and St-Fbp Mutants

Mutant	k_{cat} (s^{-1})	K_m (mM)	k_{cat}/K_m (s^{-1} mM^{-1})
Wild-type	2.5 ± 0.06	0.027 ± 0.002	735
D12A	0.054 ± 0.001	0.55 ± 0.07	0.79
H19A	4.3 ± 0.2	0.13 ± 0.02	270
D53A	0.077 ± 0.004	0.15 ± 0.02	4.2
D54A[a]	0.0024	ND	ND
Q95A	3.0 ± 0.2	0.025 ± 0.007	975
D132A	0.23 ± 0.004	0.014 ± 0.001	134
D233A[a]	0.0091	ND	ND
D234A[a]	0.0012	ND	ND

ND, not determined.
[a]Assayed with 5 mM FBP as a substrate.

cant FBPase activity at 80°C, with K_m and k_{cat} values that were both smaller than the reported values for Tk-Fbp (K_m = 0.1 mM and k_{cat} = 17 s^{-1} at 95°C) (Rashid et al., 2002) (Table 1). Reported k_{cat} values for the FBPase activity of three family IV FBPases (MJ0109, AF2372, and *P. furiosus* FBPase) are within the range of 2.7–7.0 s^{-1} at 85°C, but that of TM1415 is significantly higher (270 s^{-1} at 95°C) (Stec et al., 2000; Verhees et al., 2002). The relative molecular mass of the denatured St-Fbp was estimated to be 42 kDa by SDS-PAGE, and that of the native form to be 290 kDa by gel filtration chromatography. This indicates a homooctameric structure for the native St-Fbp, like for Tk-Fbp (Rashid et al., 2002). The effect of temperature on the FBPase activity was examined by means of a linked assay, the production of F6P being continuously measured between 25°C and 60°C, and discontinuously measured between 50°C and 100°C. St-Fbp was highly thermophilic, exhibiting maximum activity over 100°C. An Arrhenius plot exhibited a biphasic or discontinuous characteristic with a break point at 45°C (Figure 1). The Arrhenius activation energies were 125 and 43 (kJ mol^{-1}) below and above the break point, respectively. Since the break point is rather close to the marginal point of the two assay methods (continuous and discontinuous assays), the phenomenon might be an artifact. The enzyme exhibited maximum activity at pH 8.0, with apparent pK_a values at pH 7.0 and 9.0 (see Supplemental Figure S1 at http://www.structure.org/cgi/content/full/12/6/949/DC1).

Effect of Metal Ions

Generally, phosphatases require divalent cations for production of a nucleophilic hydroxyl ion, which attacks the phosphoryl group, and stabilization of the reaction intermediate (Bone et al., 1994). The effects of divalent cations on the enzyme activity were nearly identical to those on Tk-Fbp, except that St-Fbp absolutely required divalent cations such as Mg^{2+}, Zn^{2+}, or Mn^{2+}, while Tk-Fbp has been reported to be slightly active without divalent cations (Figure 2). The enzyme exhibited maximum activity (~4.2 U/mg) at ~5 mM Mg^{2+}, with a half maximum effective concentration of ~0.5 mM. Mg^{2+} did not

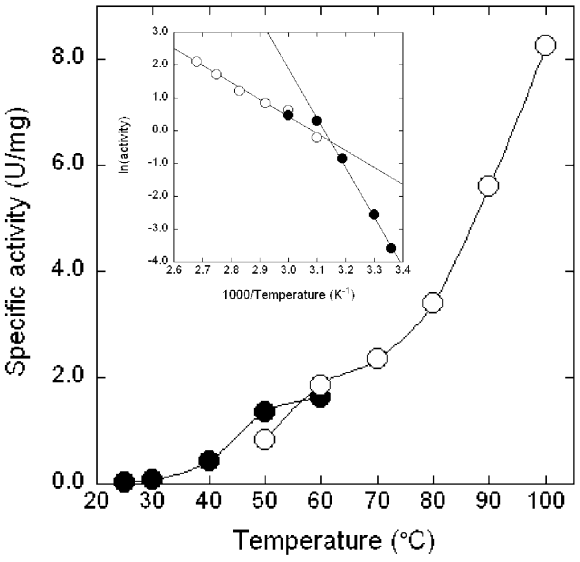

Figure 1. Effect of Temperature on the FBPase Activity of St-Fbp

The FBPase activity was continuously measured between 25°C and 60°C (closed circle), and discontinuously measured between 50°C and 100°C (open circle). The inset shows an Arrehenius plot.

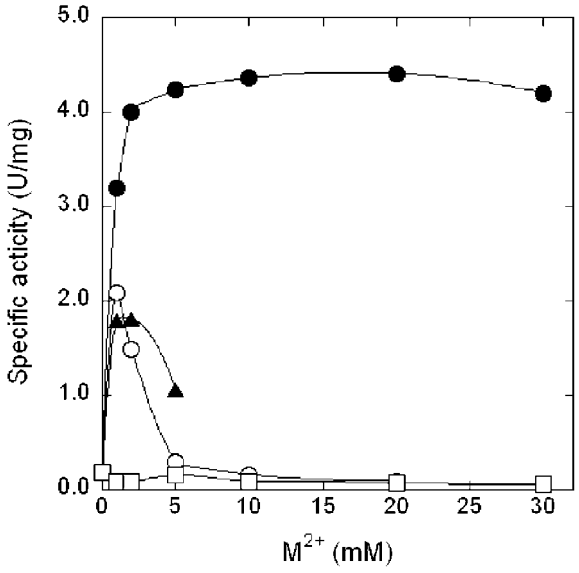

Figure 2. Effect of Divalent Metal Ions on the FBPase Activity of St-Fbp

Symbols used were as follows: Mg^{2+}, closed circle; Mn^{2+}, closed triangles; Zn^{2+}, open circles; and Ca^{2+}, open squares.

inhibit the activity, at least up to 30 mM. Zn^{2+} and Mn^{2+} ions also enhanced the enzyme activity (2.1 and 1.8 U/mg, respectively) at low concentration ($\sim$1 mM), whereas higher concentrations of both cations had an inhibitory effect. On the other hand, the Ca^{2+} ions were unable to support the enzyme activity. These results indicate that the Mg^{2+} ion is the most effective divalent cation for St-Fbp, and it seems to support the enzyme activity also in vivo.

A number of phosphotransferase enzymes including FBPase I (Zhang et al., 1996) and eukaryal/bacterial IMPases (Matsuhisa et al., 1995; McAllister et al., 1992) are known to be significantly inhibited by Li^+. Inhibition of human IMPase by Li^+ has received much attention, because it is related to the lithium therapy for manic depression (Gore et al., 1993). On the other hand, Li^+ does not strongly inhibit FBPase IV enzymes such as the *T. maritima* TM1415 (Chen and Roberts, 1999), *M. jannaschii* MJ0109 (Chen and Roberts, 1998), and *A. fulgidus* AF2372 (Stieglitz et al., 2002) ones (the IC_{50} values are 100, 250, and 290 mM, respectively). However, the FBPase IV enzyme from *P. furiosus* FBPase is significantly inhibited by Li^+ (the IC_{50} is 1 mM) (Verhees et al., 2002). Interestingly, the St-Fbp enzyme was less inhibited by Li^+ (the IC_{50} is $\sim$650 mM) compared to other known FBPases. The Na^+ ions slightly inhibited the St-Fbp activity like Li^+, while the enzyme activity increased to $\sim$135% of the basal level with 100 mM K^+.

Crystallography and Overall Structure

St-Fbp was crystallized by the oil-batch method in the presence of 2.5 mM Mg^{2+} and 2.5 mM FBP. These ligands were found to be essential for crystal formation. Divalent cations and sugar phosphates are also necessary for crystallization of MJ0109 (Stec et al., 2000). The St-Fbp crystal belonged to space group *I*422 with unit cell dimensions of a = b = 111.8 Å and c = 153.2 Å. The structure was solved by the MAD method using a crystal labeled with Se-Met, and refined to an R factor of 18.3% at 1.8 Å resolution (Table 2). As there was no observable electron density for the N-terminal 2 residues, the region between 226 and 228, and the C-terminal 21 residues, these regions were not included in the final model. The crystal contained one subunit, one FBP molecule, four metal ions (assigned as Mg^{2+}), and one 2-methyl-2,4-pentanediol (MPD) molecule per asymmetric unit. Electron density of the FBP molecule in the open-keto form was clearly visible even in the Fourier map generated with the experimental MAD phase (see Supplemental Figure S2). The monomers in the asymmetric unit are related by crystallographic 4- and 2-fold axes to generate a homooctamer of the 422 point-group (Figures 3A and 3B). The eight subunits are tightly linked to form a ring-shaped dimer of tetramers. The MPD molecule is located near the helix α7, inside the ring-shaped dimer and far from the active site (Figure 3C). St-Fbp is composed of one domain with four-layered interleaved α helices and β sheets forming an α-β-α-β-α four-layer sandwich fold (Figures 3C and 3D). A topology diagram is presented in Figure 3E.

Structural Comparison

The overall fold of St-Fbp was completely different with those of previously structural known FBPases (FBPase I [Choe et al., 2000] and IV [Stec et al., 2000]), which are organized in five layered interleaved α helices and β sheets forming an α-β-α-β-α five-layered sugar phosphatase fold (Figure 4A). A structure database search was performed using the Dali server (Holm and Sander, 1993). As to the N-terminal 115 residues of St-Fbp, four antiparallel β strands (β4, β1, β3, and β2) and two flanking α helices (α1 and α2) were found to be homologous to bovine testis acylphosphatase (Z score = 5.8, rmsd = 2.6 Å for 75 residues) (Thunnissen et al., 1997) (Figure 4B). As to the remainder C-terminal 229 residues, seven antiparallel β strands (β6, β8, β9, β10, β5, β14, and β15) and two flanking α helices (α3 and α6) are structurally similar to the C-terminal region of the β chain of S-adenosylmethionine decarboxylase (Z score = 4.5, rmsd = 3.6 Å for 97 residues) (Ekstrom et al., 1999) (Figure 4B). Since the active site of St-Fbp is located at different position from these enzymes (acylphosphatase and S-adenosylmethionine decarboxylase), there seems to be no functional relationship with them. When the database search was performed with the whole polypeptide of St-Fbp, acylphosphatase was again found to be the structurally closest protein to the N-terminal region, and there was no significantly similar structure to the whole monomer.

Active Site

The FBP molecule was bound at the subunit interface within the ring-shaped tetramer, in an open-form (keto form) (Figure 5A). The 1-phosphoryl group of the FBP molecule penetrates into the protein, and is surrounded by four Mg^{2+} ions. On the other hand, the 6-phosphate group is recognized by the adjacent subunit. The FBP molecule appears to be occluded from the solvent by the loop between α2 and β4 (Figure 5A). Average B factor of this loop (23.8 $Å^2$) was relatively higher compared with that of the whole polypeptide (19.5 $Å^2$), indicating that this loop is expected to be flexible at the high temperature in vivo. The biphasic characteristic of the Arrhenius plot for St-Fbp can be explained if the increased mobility of the loop at high temperature is required for substrate binding. Actually, FBPase V genes are only present in thermophilic organisms (Rashid et al., 2002).

The electron density map at the 1-phosphoryl group was unambiguously connected, indicating that the FBP was not hydrolyzed even under the cocrystallization conditions (Figure 5B). The average B factor of the 1-phosphoryl group (16.6 $Å^2$) is not greatly different from that of the remaining part of the FBP molecule (14.9 $Å^2$). Because this enzyme exhibits very low activity at 25°C (less than 0.01 U/mg), intact FBP seemed to remain in the crystallization solution during crystallization (about 20 hr).

The FBP molecule is located at the side of the four-layer sandwich fold and is recognized by six loop regions (β1-α1, β2-β3, α2-β4, β5-3_{10}1, β9-β10, and 3_{10}6-α8) (Figure 3C). A schematic drawing of the interactions between the enzyme and the FBP molecule is presented in Figure 5C. The residues involved in metal binding and recognition of the FBP molecule are highly conserved among FBPase V family enzymes (Figure 6). The 6-phosphoryl group is partly recognized by Gln242 and His243

Table 2. Crystallographic Data and Refinement

Data Collection Statistics				
		SeMet MAD Data[a]		
	Native FBP Complex	Edge	Peak	Remote
X-ray source	SPring8 BL-40B2	SPring8 BL-40B2		
Space group	*I*422	*I*422		
Unit cell (Å)	a = b = 111.8, c = 153.2	a = b = 111.4, c = 153.2		
Wavelength (Å)	0.9712	0.9794	0.9792	0.9712
Resolution (Å)[b]	91.3–1.8 (1.86–1.8)	91.3–2.25 (2.37–2.25)		
Number of reflections				
Measured	309,670	941,001	934,117	941,554
Unique	44,654	62,629[c]	62,549[c]	62,594[c]
Completeness (%)[b]	99.1 (99.7)	100 (100)	100 (100)	100 (100)
R_{sym} (%)[b]	4.0 (14.1)	6.8 (13.7)	7.5 (15.4)	8.7 (19.3)

Refinement Statistics	
Resolution (Å)	19.2–1.8
Number of reflections	
Total	44,654
Test set	2,212
R factor (%)	18.3
R_{free} (%)[d]	19.7
No. of protein residues	359
No. of water molecules	262
No. of FBP molecule	1
No. of Mg ions	4
No. of MPD molecule	1
Ramachandran plot (%)	
Most favored	88.1
Allowed	11.9
Disallowed	0
Average B factor (Å^2)	20.5
Rmsd from ideal values	
Bond lengths (Å)	0.011
Bond angles (degree)	1.6

[a] MAD datasets were collected from a crystal in the complex form with FBP.
[b] Values in parentheses are for the highest resolution shell.
[c] For the MAD data sets, Friedel pairs were counted as independent.
[d] Calculated using a test data set; 5% of total data randomly selected from the observed reflections.

at the loop between β10 and α6 of the adjacent subunit (Figures 3C and 5A). The FBP molecule is recognized by a number of polar interactions. The four oxygen atoms of the 1-phosphate group are liganded to four Mg^{2+} ions and are located within hydrogen-bonding distance to Asp12, His19, Asp53, Gln95, Asn105, Asp132, Lys133, Asp234, Wat1, Wat3, Wat4, and Wat5. The 3-hydroxyl group forms hydrogen bonds with Arg266 and Asp287. The 4-hydroxyl group forms a hydrogen bond with Tyr348. The 5-hydroxyl group interacts with Asp287 and Gln242 of the adjacent subunit through hydrogen bonds. The 6-phosphate moiety maintains a hydrogen-bonding network with His19, Tyr91, Gly104 and Tyr348, and Gln242 and His243 from the adjacent subunit.

The four Mg^{2+} atoms around the 1-phosphoryl group showed good electron density peaks in shape (Figure 5B), and the B factors were refined to usual values (17.0, 18.2, 7.75, and 9.98 Å^2 for Mg1–4, respectively). All of the four Mg^{2+} ions are octahedrally hexacoordinated (Figure 5D and Table 3). However, the coordination of Mg1 is distorted, the distance between Mg1 and FBP O1 atom being 2.7 Å, and the distance between Mg1 and Asp233 being 1.9 Å. To confirm that these peaks are not originated form other divalent cations, Mn^{2+} and Zn^{2+} ions were placed at the Mg1–4 positions of the model as a test. Refined B factors of the putative Mn^{2+} and Zn^{2+} ions were rather high (all above 23.4 and 29.8 Å^2). Refined F_o-F_c electron density maps with Mn^{2+} and Zn^{2+} ions still exhibit negative peaks ($<-4\ \sigma$) at the metal binding sites, whereas that with Mg^{2+} ions was almost flat (see Supplemental Figure S3).

One water molecule (Wat1) exhibits in-line geometry with respect to the 1-phosphoryl group, where Wat1 can attack the phosphorous atom with the assistance of Mg2 and Mg3. This water molecule is liganded to the Mg2 and Mg3 atoms, and located within hydrogen-bonding distance to Asp12, Asp53, Asp54, and the water (Wat7) liganded to Mg2. The kinetic parameters of the mutants at metal-coordinating residues are shown in Table 1. The k_{cat} values of the H19A and Q95A mutants were slightly elevated, indicating that Mg4 is not essential for catalysis. The significantly elevated K_m value of the H19A mutant indicates the importance of this residue for substrate binding. The side chain of His19 provides an aromatic core, which is surrounded by the slightly rounded FBP molecule (Figure 5A). Moreover, the two side chain nitrogen atoms form hydrogen bonds with the 1- and 6-phosphoryl groups of the FBP molecule.

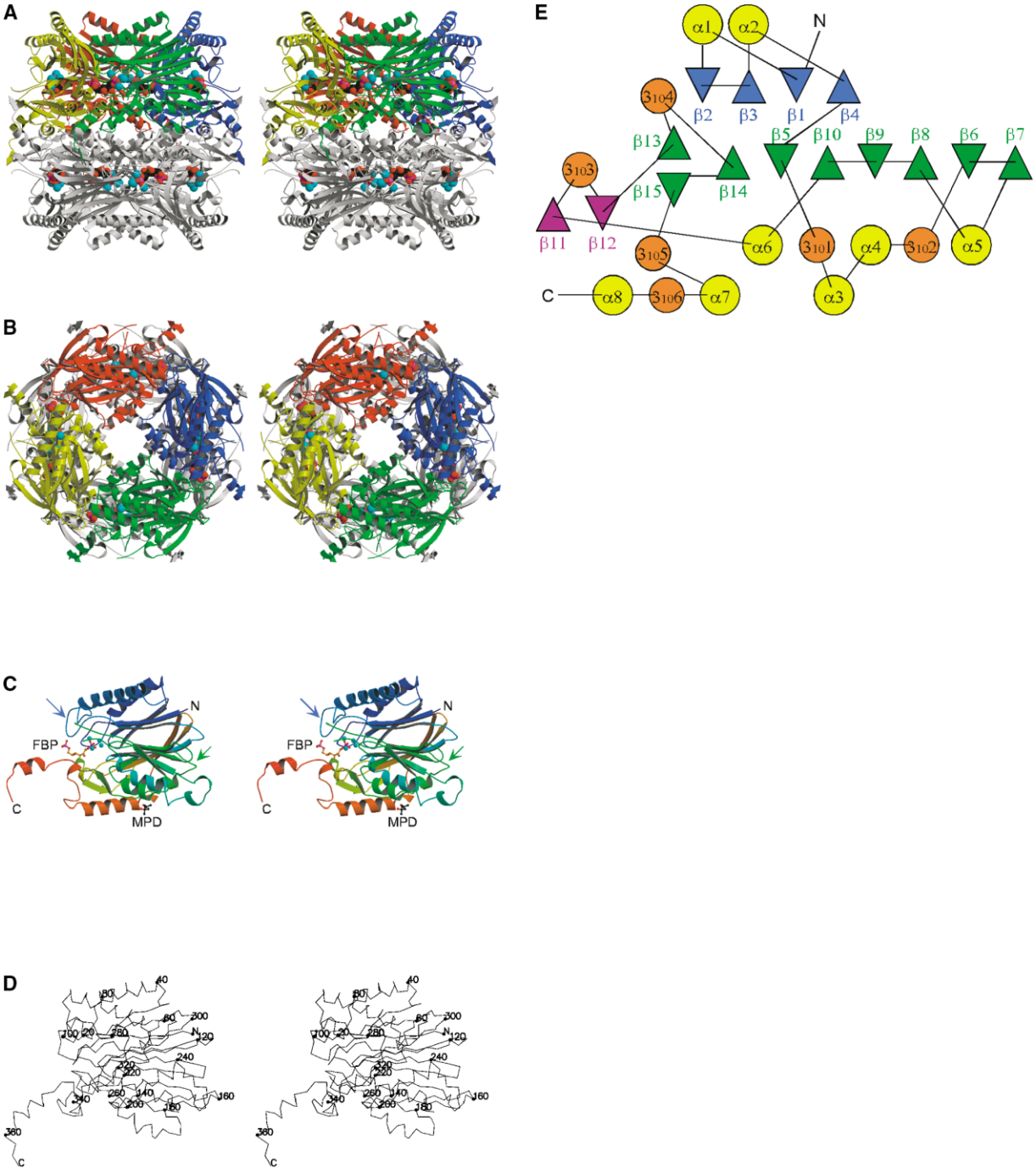

Figure 3. Overall Structure of St-Fbp

(A) Stereoview of the diagram of the octamer structure. Each monomer in one tetramer is shown in different colors, and monomers in the other tetramer in white. FBP molecules (carbon, black; oxygen, red; and phosphorus, magenta) and magnesium ions (cyan) are depicted as space-filling models. The monomers in the asymmetric unit are related by crystallographic 4- and 2-fold axes to generate a homooctamer of the 422 point-group.

(B) The view rotated 90° around the horizontal axis from that in (A).

(C) Stereoview of a ribbon diagram of the monomer structure, colored from blue at the N terminus to red at the C terminus. FBP and MPD molecules are depicted as ball-and-stick models, and magnesium ions (cyan) are presented as space-filling models. The loop between α2 and β4 is indicated by the blue arrow. The loop between β10 and α6, which recognizes the 6-phosphoryl group of FBP in the adjacent subunit, is indicated by the green arrow.

(D) Stereoview of a Cα trace of a St-Fbp monomer, with every 20th amino acid numbered and presented as a sphere.

(E) Topology diagram of St-Fbp. α- and 3_{10} helices are shown as yellow and orange circles, respectively. β strands are shown as blue, green, and magenta triangles.

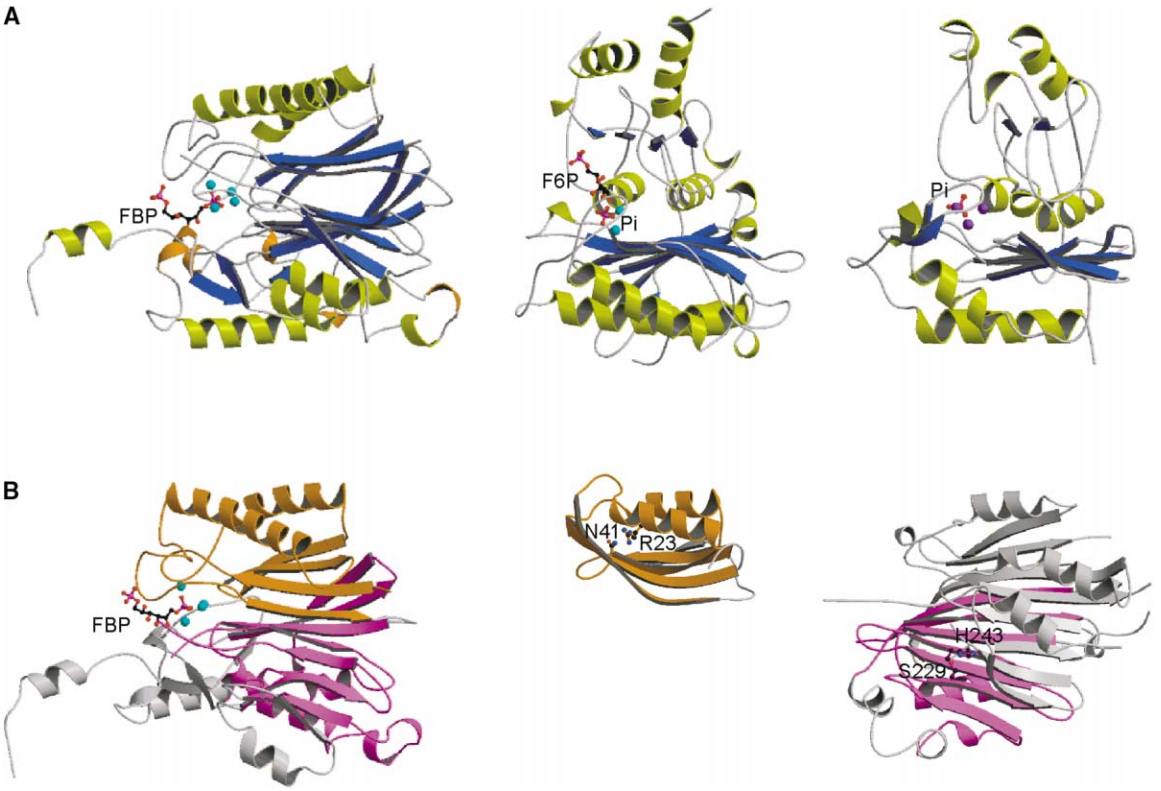

Figure 4. Structural Comparison

(A) The overall structure of St-Fbp (left), FBPase I (pig kidney FBPase, PDB code 1EYI; middle), and FBPase IV (MJ0109, PDB code 1DK4; right). FBP, F6P, and Pi molecules are depicted as ball-and-stick models. Magnesium (cyan) and zinc (purple) ions are presented as space-filling models. α and 3_{10} helices are shown in yellow and orange, and β strands in blue, respectively.

(B) The overall structure of St-Fbp, with acylphosphatase-like domain colored orange and S-adenosylmethionine decarboxylase-like domain colored magenta (left). The overall structure of acylphosphatase (PDB code 2ACY) with St-Fbp-like region colored orange and catalytic residues, Arg23 and Asn41, shown as ball-and-stick models (middle). The overall structure of S-adenosylmethionine decarboxylase (PDB code 1JEN) with St-Fbp-like domain colored magenta and catalytic residues, Ser229 and Arg243, shown as ball-and-stick models (right).

On the other hand, mutants of the residues coordinating Mg1–3, as well as the D12A mutant, exhibited severe decreases in k_{cat}. These results indicate that Mg1–3 are essential for catalysis.

Catalytic Mechanism

The arrangement of the catalytic side chains and metal ligands in the active site of St-Fbp is consistent with associative three-metal ion assisted catalysis (Figure 7), which is proposed for FBPase I (Choe et al., 2003b) and also for FBPase IV (Johnson et al., 2001). The water molecule (Wat1) coordinated by both Mg2 and Mg3 appears to have the right environment for deprotonation and the creation of a hydroxide, which could serve as the primary nucleophile. Asp12, Asp53, or the water molecule (Wat7) liganded to Mg2 can serve as a base to accept the proton from Wat1. Of these candidates, Asp12 is the most promising one; because the D12A mutant exhibited severely decreased catalytic activity despite it being liganded to the catalytically irrelevant Mg4. This nucleophilic water molecule would approach the phosphate in an in-line attack. Mg1 should serve to stabilize the developing negative charge on the phosphate oxygen. The significantly distant location of Mg1 from FBP O1 in the present crystal structure may stabilize the FBP-complex form. The dissociative mechanism, in which a phosphate ester is hydrolyzed through an intermediate of metaphosphate (Choe et al., 2003a), also seems to be possible, but there is no evidence at present. The detailed catalytic mechanism of St-Fbp remains to be elucidated.

The most interesting feature of the St-Fbp structure is the FBP molecule bound in the open-keto form at the active site. All of the currently reported complex structures of FBPases contain a closed-ring form of FBP or F6P. It is not clear whether or not the ring opening is catalytically assisted, as observed for sugar isomerases (Allen et al., 1994; Lee et al., 2001). However, we could not find definitive catalytic factor for the sugar-ring opening in the St-Fbp structure. Mg4 and His19 appear to be able to assist the sugar-ring opening catalysis, because they are located near the FBP molecule. However, this possibility is denied since the H19A and Q95A mutants retained full activity. Moreover, we could not find appropriate space in the active site that can accommodate the closed form of FBP, nor the putative binding sites for the two phosphoryl groups, which would become closer in the closed form. A large conformational rearrangement must be assumed if the enzyme can cat-

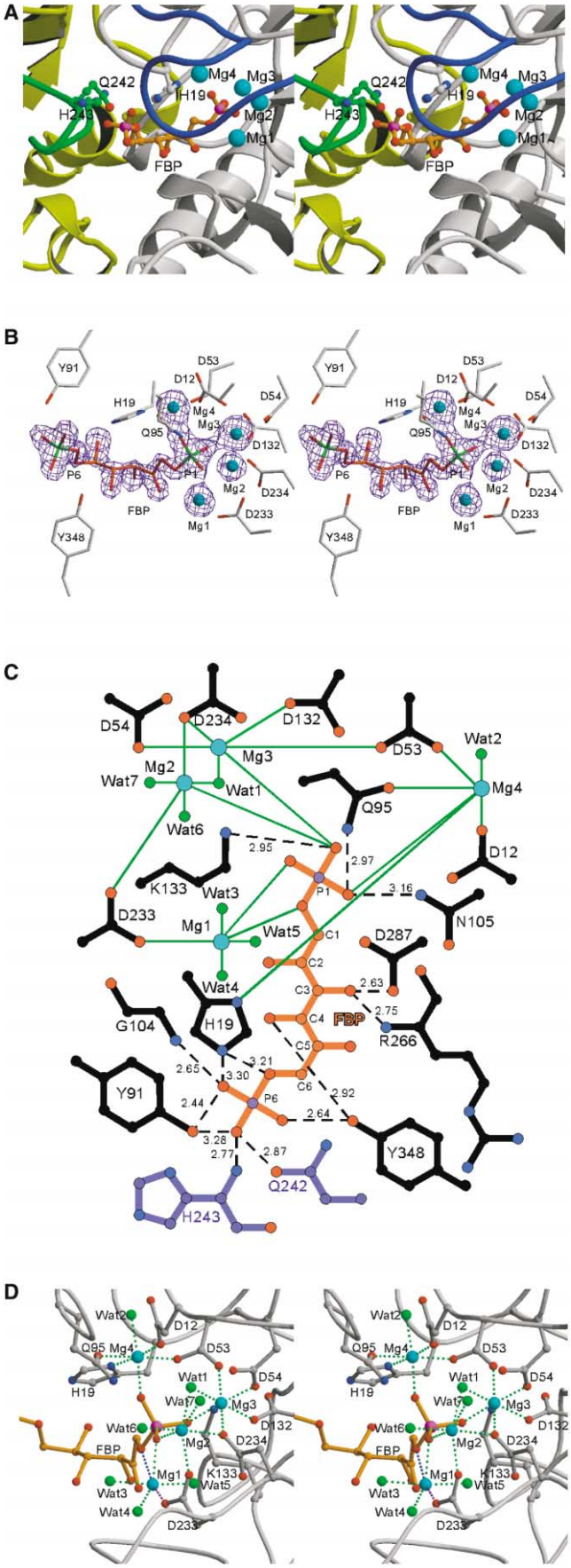

Figure 5. The Active Site of St-Fbp

(A) Stereoview of the dimer interface of St-Fbp. FBP molecule is depicted as ball-and-stick model, and magnesium ions (cyan) are presented as space-filling models. A monomer is shown in white, and the loop between α2 and β4 in blue. The adjacent monomer is shown in yellow, and the loop between β10 and α6, which recognizes the 6-phosphoryl group of FBP, is shown in green.

(B) Stereoview of the Fo-Fc omit electron density maps contoured at 6 σ at the active site of St-Fbp. The map was calculated using the phase of a model structure without FBP molecule and Mg atoms.

(C) Schematic drawing of interactions between the enzyme and the FBP molecule. Amino acid residues from the adjacent subunit are shown in purple. The coordination of Mg^{2+} ions is shown as green lines. Hydrogen bonds are indicated by dashed black lines and lengths are given in angstroms. For clarity, hydrogen bonds between the FBP molecule and the residues coordinated by Mg^{2+} ions are omitted.

(D) Stereoview of the metal binding site of St-Fbp. FBP molecule is depicted as ball-and-stick model, and magnesium ions (cyan) and water molecules (green) are presented as space-filling models. The coordination between Mg1 and the FBP O1 atom (2.7 Å), and that between Mg1 and Asp233 (1.9 Å) are shown by blue and purple dashed lines, respectively.

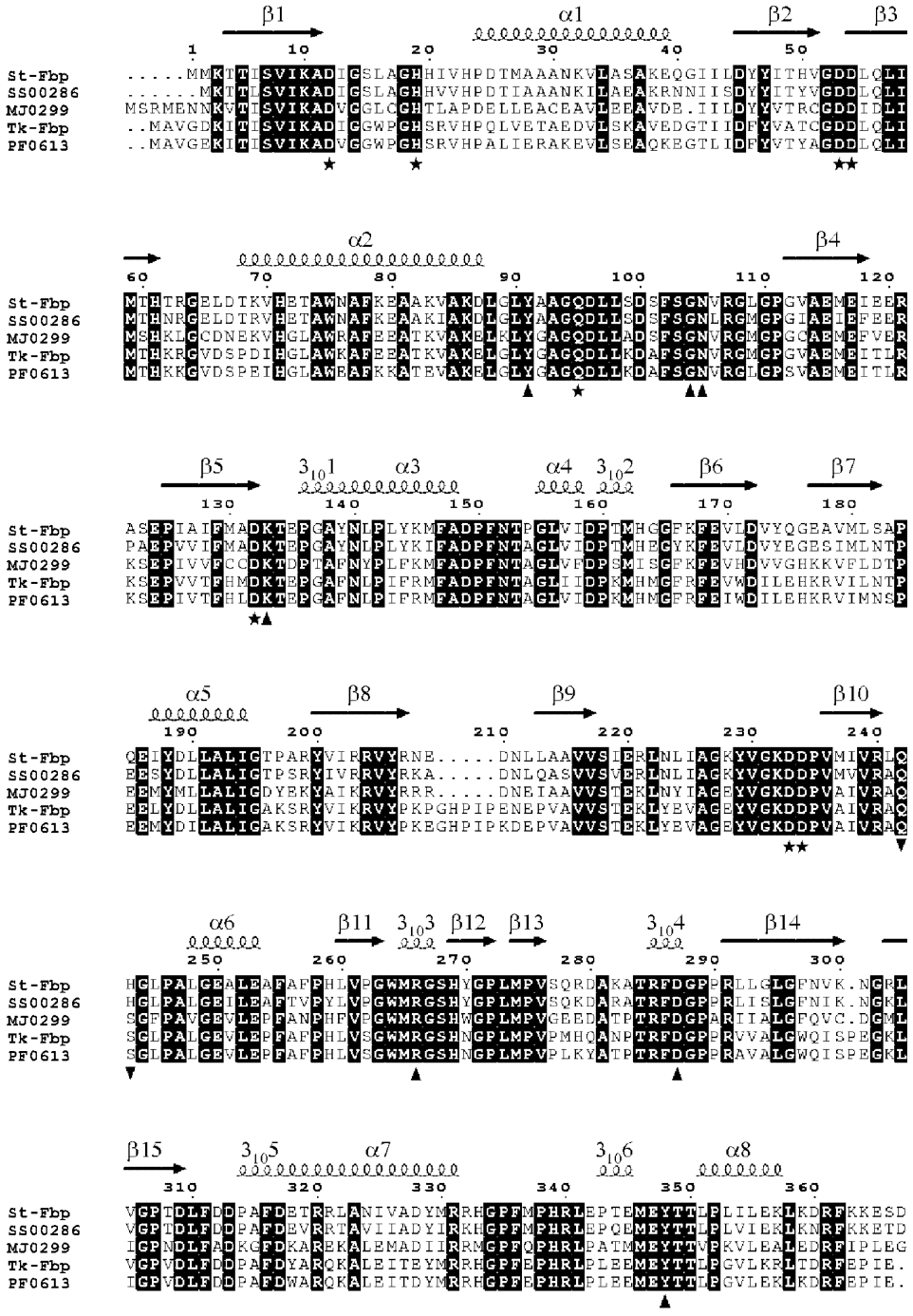

Figure 6. Amino Acid Sequence Alignment of the FBPase V Family

Identical residues are highlighted in black. The residues involved in metal binding and recognition of a substrate are indicated by stars and upward-pointing triangles, respectively. The residues interacting with a substrate from the adjacent subunit are indicated by downward-pointing triangles. St-Fbp, FBPase (*Sulfolobus tokodaii* strain 7 ORF ST0318); SS0286, *Sulfolobus solfataricus* ORF SS0286; MJ0299, *Methanococcus jannaschii* ORF MJ0299; Tk-Fbp, *Thermococcus kodakaraensis* KOD1 FBPase (AB081839); and PF0613, *Pyrococcus furiosus* ORF PF0613. The sequences were aligned with CLUSTAL W (Thompson et al., 1994), and the secondary structure of St-Fbp was assigned with DSSP (Kabsch and Sander, 1983).

alyze the sugar-ring opening. Therefore, we currently conclude that St-Fbp catalyzes the hydrolysis of the open-keto form of FBP, which is present 2.0% fraction in solution at room temperature (Midelfort et al., 1976). At the extreme temperatures in which thermophilic organisms exist, the equilibrium would shift to the entropically favorable open form. The nonenzymatic ring-opening rates for FBP in solution at pH 7.2 and 25°C are 8 and

Table 3. Metal Binding Sites of St-Fbp

Metal-Ligand Distances (Å)							
Site 1 (Mg1)		Site 2 (Mg2)		Site 3 (Mg3)		Site 4 (Mg4)	
Oδ2 Asp233	1.90	Oδ1 Asp233	2.26	Oδ1 Asp53	2.10	Oδ2 Asp12	2.08
O11 FBP	2.16	Oδ2 Asp234	2.38	Oδ1 Asp54	2.15	Nδ1 His19	2.20
O1 FBP	(2.72)	O11 FBP	2.28	Oδ1 Asp132	2.09	Oδ2 Asp53	2.10
O (Wat3)	2.16	O (Wat1)	2.44	Oδ1 Asp234	2.03	Oε1 Gln95	2.29
O (Wat4)	2.06	O (Wat6)	2.37	O12 FBP	2.16	O13 FBP	2.01
O (Wat5)	2.16	O (Wat7)	2.35	O (Wat1)	2.11	O (Wat2)	2.02

35 s^{-1} for the α and β anomers, respectively (Midelfort et al., 1976). These values are larger than the k_{cat} value of St-Fbp at 80°C (2.5 s^{-1}). It is suggested that thermophilic phosphoglucose isomerase (PGI) from *P. furiosus*, in which a residue acting as an acid catalyst in ring-opening is absent, has specificity for substrates in the strait chain form, while conventional PGIs catalyze sugar ring opening (Swan et al., 2003).

Implications for Li^+ Inhibition

It is proposed that the Li^+ ion bound to the Mg^{2+} binding site in the active center of human IMPase inhibits its catalysis and subsequent release of the reaction product (Bone et al., 1994). A loop forming the active site of the Li^+-insensitive sugar phosphatases is found to be relatively short, thus its active site is closed compared with the Li^+-sensitive ones (Steiglitz et al., 2002). Because the overall structure of St-Fbp is completely different from those of FBPases I and IV, it is not possible to compare their active site structures by superimposition. However, the active center of St-Fbp looks clearly more closed than those of FBPases I and IV (Figure 4A). The 1-phosphoryl group of the FBP molecule deeply penetrates into the active site pocket of St-Fbp, and occluded from the solvent by the loop α2-β4 (Figure 5A). The structural difference seems to cause the weakest inhibition of St-Fbp by Li^+ among the sugar phosphatases examined so far.

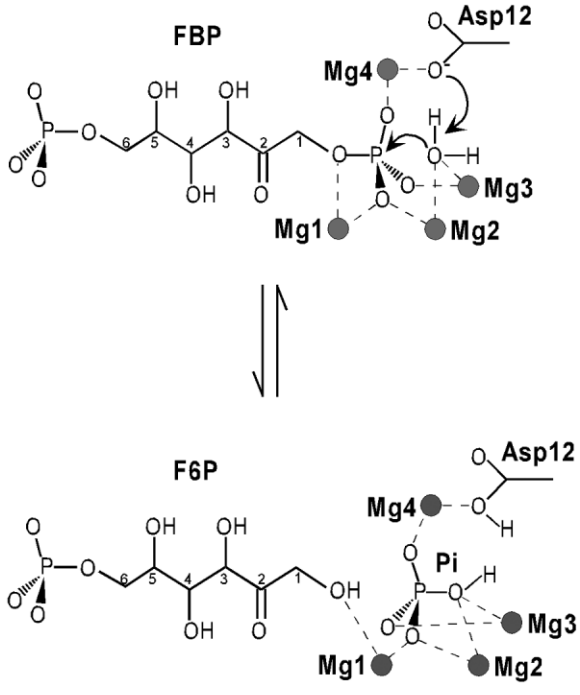

Figure 7. Proposed Catalytic Mechanism of St-Fbp

The open form of FBP binds to the active site of St-Fbp. Asp12 likely abstracts the proton from the water molecule coordinated by both Mg2 and Mg3, creating a hydroxide anion as the primary nucleophile. The hydroxide anion would approach the phosphate in an in-line attack, generating F6P and Pi.

Concluding Remarks

The first crystal structure of FBPase V reported here revealed the novel fold of the sugar phosphatase, and a similar catalytic mechanism to those of other classes of FBPases. It also provided an insight into the structural basis of the strict substrate specificity for FBP. FBPase V does not exhibit IMPase activity, because the sugar alcohol IMP cannot take on the open form. It is interesting that two types of FBPases with different substrate specificities and comparable catalytic activities are present in thermophilic archaea. Further investigation on the regulation of the two genes and the gene products will reveal their roles in vivo.

Experimental Procedures

Expression and Purification

The gene encoding FBPase (ST0318) of *S. tokodaii* strain 7 was amplified by PCR and then inserted between the NdeI and EcoRI sites of the pET17b expression vector (Novagen) to construct plasmid pStFbp. The primers used were 5′-GTAATAAG*CATATG*AT GAAAACTACTATAAGTG-3′ and 5′-AAA*GAATTC*ATTAATCATGAC CTTGACTTTC-3′, the NdeI and EcoRI sites being in italic, respectively. *E. coli* BL21(DE3) (Novagen) cells harboring plasmid pStFbp were grown in Luria-Bertani (LB) medium containing 100 mg/l of ampicillin for 20 hr at 37°C. After cultivation, the cells were harvested and resuspended in 20 mM Tris-Cl (pH 8.0) containing 0.1 mM phenylmethylsulfonyl fluoride (PMSF). The cell suspension was sonicated, incubated for 30 min at 80°C, and then centrifuged. The supernatant containing the target protein was purified by Q-Sepharose Fast Flow, Superdex 200 HR 10/30, and Mono Q HR 5/5 (Pharmacia) column chromatographies. The purified enzyme was dialyzed against 5 mM Tris-Cl (pH 7.0) and then concentrated. The protein concentration was determined with a bicinchoninic acid (BCA) protein assay kit (Pierce) using bovine serum albumin as a standard. The selenomethionine-substituted enzyme was expressed in methionine auxotroph *E. coli* B834 (DE3) (Novagen) in Se-Met core medium (Wako) supplemented with 10 g/l D-glucose, 250 mg/l $MgSO_4 \cdot 7H_2O$, 4.2 mg/l $FeSO_4 \cdot 7H_2O$, 8.3 μl/l H_2SO_4, 10 ml/l Vitamino growth supplement (Sigma), 100 mg/l ampicillin, and 25 mg/l seleno-L-methionine (Wako). The purification procedures were the same as those for the native enzyme.

Crystallization and Data Collection

Crystals were grown within a day at 25°C under Al's Oil (Hampton) using the microbatch technique. Native FBP-complex crystals were obtained by mixing 5 μl of a protein solution (15 mg /ml) with an equal volume of a crystallization solution comprising 0.1 M Tris-Cl (pH 8.2), 13% (w/v) PEG 8000, 5 mM $MgCl_2$, 0.1 M NaCl, and 5 mM FBP. Selenomethionine-substituted FBP complexes were obtained in the same way as the native ones, except that 9% (w/v) PEG 3350 was used instead of 13% (w/v) PEG 8000 as the precipitant. Crystals were flash-frozen in crystallization buffer supplemented with 25% MPD. The multiple wavelength anomalous diffraction (MAD) data set for a selenomethionine-substituted crystal was collected at wavelengths of 0.9794 Å (edge), 0.9792 Å (peak), and 0.9712 Å (remote), and the native data set for the FBP complex was collected at a wavelength of 0.9712 Å with the beamline BL40B2 of SPring-8 (Hyogo, Japan), respectively. Data collection was performed at 100 K. The data sets were processed with the HKL2000 program suite (Otwinowski and Minor, 1997).

Structure Determination and Refinement

The phase calculations were carried out with program SOLVE (Terwilliger and Berendzen, 1999) based on the MAD data set, and 13 out of 14 potential selenium sites were identified. Program ARP/wARP (Perrakis et al., 1999) was used for automatic model building. The resulting model was used as the starting model to refine the native data sets at a higher resolution. Using program XtalView (McRee, 1999), manual refitting of the models was performed. Energy minimization and individual B factor refinement were carried out with program CNS (Brünger et al., 1998). The stereochemistry of the protein model was analyzed with PROCHECK (Laskowski et al., 1996). The figures were prepared with Raster3D (Merritt and Murphy, 1994), MOLSCRIPT (Kraulis, 1991), XtalView (McRee, 1999), LIGPLOT (Wallace et al., 1995), and ESPript (Gouet et al., 1999).

Site-Directed Mutagenesis and Enzyme Assay

Site-directed mutagenesis was performed with a QuikChange site-directed mutagenesis kit (Stratagene). The wild-type and all mutant proteins were expressed in *E. coli* BL21(DE3), and purified by heat treatment at 80°C for 30 min, and Q-Sepharose Fast Flow and Superdex 200 HR 10/30 column chromatographies to apparent homogeneity, as judged on SDS-PAGE. The purified enzymes were dialyzed against 20 mM Tris-Cl (pH 7.0) and then concentrated. FBPase activity was determined by means of a spectrophotometric, coupled enzyme assay (Riou et al., 1977). One unit of enzyme activity was defined as the amount of enzyme that catalyzed the formation of 1 μmol of NADPH per minute. Production of F6P was continuously measured between 25°C and 60°C, and discontinuously measured between 50°C and 100°C. All buffers used for assays were prepared at room temperature. A standard reaction mixture (300 μl) comprising 0.1 M HEPES-Na (pH 8.0), 10 mM $MgCl_2$, 2 mM FBP, and 10 μl of enzyme solution was used for assays between 50°C and 100°C. The reaction mixture without the enzyme solution (290 μl) was preincubated at temperatures varying from 50°C to 100°C for ~2 min and then the reaction was initiated by the addition of 10 μl of enzyme solution. At different times up to 2 min, the reaction was stopped by quickly chilling the mixture on ice, and then the coupling enzyme solution (100 μl) comprising 0.1 M HEPES-Na (pH 8.0), 10 mM $MgCl_2$, 0.4 mM $NADP^+$, 0.4 U phosphoglucose isomerase (PGI), and 0.4 U glucose-6-phosphate dehydrogenase (G6PDH) was added to start the coupling reaction. After incubation at 25°C for 30 min, the generation of NADPH was monitored at 340 nm. A reaction mixture (400 μl) composed of 0.1 M HEPES-Na (pH 8.0), 10 mM $MgCl_2$, 2 mM FBP, 0.4 mM $NADP^+$, 0.4 U PGI, 0.4 U G6PDH, and FBPase was used for assays between 25°C and 60°C, with continuous monitoring at 340 nm at the desired temperature. For examination of the effect of pH on the FBPase activity, assays were continuously performed at 60°C with 100 mM of the following buffers: acetate-Na (pH 4.5–5.5), MES-Na (pH 5.5–7.0), HEPES-Na (pH 7.0–8.0), BICINE-Na (pH 8.0–9.0), and CHES-Na (pH 9.0–10).

The effects of monovalent cations (Li^+, Na^+, and K^+) and divalent cations (Mg^{2+}, Mn^{2+}, Zn^{2+}, and Ca^{2+}) on the FBPase activity were investigated at 80°C using the standard reaction mixture supplemented with a monovalent cation (20–500 mM), and the standard reaction mixture with 10 mM $MgCl_2$ replaced by a divalent cation (1–30 mM), respectively. To determine the kinetic parameters, the substrate concentration was varied from 0.01 to 5 mM, the enzyme concentrations used for the assaying of the wild-type, and D12A, H19A, D53A, D54A, Q95A, D133A, D233A, and D234A mutant enzymes being 4.7, 130, 6.9, 37, 220, 4.6, 55, 200, and 260 μg/ml, respectively. Kinetic characterization was performed at 80°C. The steady-state kinetic data were analyzed with Kaleidagraph (Synergy) software.

Acknowledgments

We wish to thank Dr. K. Miura and the staff of SPring-8 for the data collection. The synchrotron radiation experiments were performed at SPring-8 with the approval of the Japan Synchrotron Radiation Research Institute (JASRI) (Proposal No. 2002B804-RL1). This work was supported by the National Project on Protein Structural and Functional Analysis.

Received: November 21, 2003
Revised: November 23, 2003
Accepted: March 10, 2004
Published: June 8, 2004

References

Allen, K.N., Lavie, A., Glasfeld, A., Tanada, T.N., Gerrity, D.P., Carlson, S.C., Farber, G.K., Petsko, G.A., and Ringe, D. (1994). Role of the divalent metal ion in sugar binding, ring opening, and isomerization by D-xylose isomerase: replacement of a catalytic metal by an amino acid. Biochemistry *33*, 1488–1494.

Bone, R., Frank, L., Springer, J.P., and Atack, J.R. (1994). Structural studies of metal binding by inositol monophosphatase: evidence for two-metal ion catalysis. Biochemistry *33*, 9468–9476.

Brünger, A.T, Adams, P.D., Clore, G.M., DeLano, W.L., Gros, P., Grosse-Kunstleve, R.W., Jiang, J.S., Kuszewski, J., Nilges, M., Pannu, N.S., et al. (1998). Crystallography & NMR system: a new software suite for macromolecular structure determination. Acta Crystallogr. D Biol. Crystallogr. *54*, 905–921.

Chen, L., and Roberts, M.F. (1998). Cloning and expression of the inositol monophosphatase gene from *Methanococcus jannaschii* and characterization of the enzyme. Appl. Environ. Microbiol. *64*, 2609–2615.

Chen, L., and Roberts, M.F. (1999). Characterization of a tetrameric inositol monophosphatase from the hyperthermophilic bacterium *Thermotoga maritima*. Appl. Environ. Microbiol. *65*, 4559–4567.

Choe, J.Y., Fromm, H.J., and Honzatko, R.B. (2000). Crystal structures of fructose 1,6-bisphosphatase: mechanism of catalysis and allosteric inhibition revealed in product complexes. Biochemistry *39*, 8565–8574.

Choe, J.Y., Iancu, C.V., Fromm, H.J., and Honzatko, R.B. (2003a). Metaphosphate in the active site of fructose-1,6-bisphosphatase. J. Biol. Chem. *278*, 16015–16020.

Choe, J.Y., Nelson, S.W., Fromm, H.J., and Honzatko, R.B. (2003b). Interaction of Tl^+ with product complexes of fructose-1,6-bisphosphatase. J. Biol. Chem. *278*, 16008–16014.

De Rosa, M., Gambacorta, A., Nicolaus, B., Giardina, P., Poerio, E., and Buonocore, V. (1984). Glucose metabolism in the extreme thermoacidophilic archaebacterium *Sulfolobus solfataricus*. Biochem. J. *224*, 407–414.

DeFronzo, R.A. (1999). Pharmacologic therapy for type 2 diabetes mellitus. Ann. Intern. Med. *131*, 281–303.

Donahue, J.L., Bownas, J.L., Niehaus, W.G., and Larson, T.J. (2000). Purification and characterization of glpX-encoded fructose *1*, 6-bisphosphatase, a new enzyme of the glycerol 3-phosphate regulon of *Escherichia coli*. J. Bacteriol. *182*, 5624–5627.

Ekstrom, J.L., Mathews, I.I., Stanley, B.A., Pegg, A.E., and Ealick, S.E. (1999). The crystal structure of human S-adenosylmethionine decarboxylase at 2.25 Å resolution reveals a novel fold. Structure *7*, 583–595.

Gore, M.G., Greasley, P., McAllister, G., and Ragan, C.I. (1993). Mammalian inositol monophosphatase: the identification of residues important for the binding of Mg^{2+} and Li^{+} ions using fluorescence spectroscopy and site-directed mutagenesis. Biochem. J. *296*, 811–815.

Gouet, P., Courcelle, E., Stuart, D.I., and Metoz, F. (1999). ESPript: analysis of multiple sequence alignments in PostScript. Bioinformatics *15*, 305–308.

Holm, L., and Sander, C. (1993). Protein structure comparison by alignment of distance matrices. J. Mol. Biol. *233*, 123–138.

Johnson, K.A., Chen, L., Yang, H., Roberts, M.F., and Stec, B. (2001). Crystal structure and catalytic mechanism of the MJ0109 gene product: a bifunctional enzyme with inositol monophosphatase and fructose 1,6-bisphosphatase activities. Biochemistry *40*, 618–630.

Kabsch, W., and Sander, C. (1983). Dictionary of protein secondary structure: pattern recognition of hydrogen-bonded and geometrical features. Biopolymers *22*, 2577–2637.

Kawarabayasi, Y., Hino, Y., Horikawa, H., Jin-no, K., Takahashi, M., Sekine, M., Baba, S., Ankai, A., Kosugi, H., Hosoyama, A., et al. (2001). Complete genome sequence of an aerobic thermoacidophilic crenarchaeon, *Sulfolobus tokodaii* strain7. DNA Res. *8*, 123–140.

Konig, H., Skorko, R., Zillig, W., and Reiter, W.D. (1982). Glycogen in Thermoacidophilic Archaebacteria of the Genera *Sulfolobus*, *Thermoproteus*, *Desulfurococcus* and *Thermococcus*. Arch. Microbiol. *132*, 297–303.

Kraulis, P.J. (1991). MOLSCRIPT: a program to produce both detailed and schematic plots of protein structures. J. Appl. Crystallogr. *24*, 946–950.

Laskowski, R.A., Rullmannn, J.A., MacArthur, M.W., Kaptein, R., and Thornton, J.M. (1996). AQUA and PROCHECK-NMR: programs for checking the quality of protein structures solved by NMR. J. Biomol. NMR *8*, 477–486.

Lee, J.H., Chang, K.Z., Patel, V., and Jeffery, C.J. (2001). Crystal structure of rabbit phosphoglucose isomerase complexed with its substrate D-fructose 6-phosphate. Biochemistry *40*, 7799–7805.

Matsuhisa, A., Suzuki, N., Noda, T., and Shiba, K. (1995). Inositol monophosphatase activity from the *Escherichia coli* suhB gene product. J. Bacteriol. *177*, 200–205.

McAllister, G., Whiting, P., Hammond, E.A., Knowles, M.R., Atack, J.R., Bailey, F.J., Maigetter, R., and Ragan, C.I. (1992). cDNA cloning of human and rat brain myo-inositol monophosphatase. Expression and characterization of the human recombinant enzyme. Biochem. J. *284*, 749–754.

McRee, D.E. (1999). XtalView/Xfit: a versatile program for manipulating atomic coordinates and electron density. J. Struct. Biol. *125*, 156–165.

Merritt, E.A., and Murphy, M.E.P. (1994). Raster3d version-2.0. A program for photorealistic molecular graphics. Acta Crystallogr. D Biol. Crystallogr. *50*, 869–873.

Midelfort, C.F., Gupta, R.K., and Rose, I.A. (1976). Fructose 1,6-bisphosphate: isomeric composition, kinetics, and substrate specificity for the aldolases. Biochemistry *15*, 2178–2185.

Otwinowski, Z.M., and Minor, W. (1997). Processing of X-ray diffraction data collected in oscillation mode. Methods Enzymol. *276*, 307–326.

Perrakis, A., Morris, R., and Lamzin, V.S. (1999). Automated protein model building combined with iterative structure refinement. Nat. Struct. Biol. *6*, 458–463.

Rashid, N., Imanaka, H., Kanai, T., Fukui, T., Atomi, H., and Imanaka, T. (2002). A novel candidate for the true fructose-1,6-bisphosphatase in archaea. J. Biol. Chem. *277*, 30649–30655.

Riou, J.P., Claus, T.H., Flockhart, D.A., Corbin, J.D., and Pilkis, S.J. (1977). In vivo and in vitro phosphorylation of rat liver fructose-1, 6-bisphosphatase. Proc. Natl. Acad. Sci. USA *74*, 4615–4619.

Shieh, H.L., and Chiang, H.L. (1998). In vitro reconstitution of glucose-induced targeting of fructose-1, 6-bisphosphatase into the vacuole in semi-intact yeast cells. J. Biol. Chem. *273*, 3381–3387.

Stec, B., Yang, H., Johnson, K.A., Chen, L., and Roberts, M.F. (2000). MJ0109 is an enzyme that is both an inositol monophosphatase and the "missing" archaeal fructose-1,6-bisphosphatase. Nat. Struct. Biol. *7*, 1046–1050.

Stieglitz, K.A., Johnson, K.A., Yang, H., Roberts, M.F., Seaton, B.A., Head, J.F., and Stec, B. (2002). Crystal structure of a dual activity IMPase/FBPase (AF2372) from *Archaeoglobus fulgidus*. The story of a mobile loop. J. Biol. Chem. *277*, 22863–22874.

Swan, M.K., Solomons, J.T., Beeson, C.C., Hansen, T., Schonheit, P., and Davies, C.. (2003). Structural evidence for a hydride transfer mechanism of catalysis in phosphoglucose isomerase from *Pyrococcus furiosus*. J. Biol. Chem. *47*, 47261–47268.

Terwilliger, T.C., and Berendzen, J. (1999). Automated MAD and MIR structure solution. Acta Crystallogr. D Biol. Crystallogr. *55*, 849–861.

Thompson, J.D., Higgins, D.G., and Gibson, T.J. (1994). CLUSTAL W: improving the sensitivity of progressive multiple sequence alignment through sequence weighting, position-specific gap penalties and weight matrix choice. Nucleic Acids Res. *22*, 4673–4680.

Thunnissen, M.M., Taddei, N., Liguri, G., Ramponi, G., and Nordlund, P. (1997). Crystal structure of common type acylphosphatase from bovine testis. Structure *5*, 69–79.

Verhees, C.H., Akerboom, J., Schiltz, E., de Vos, W.M., and van der Oost, J. (2002). Molecular and biochemical characterization of a distinct type of fructose-1,6-bisphosphatase from *Pyrococcus furiosus*. J. Bacteriol. *184*, 3401–3405.

Verhees, C.H., Kengen, S.W., Tuininga, J.E., Schut, G.J., Adams, M.W., de Vos, W.M., and van der Oost, J. (2003). The unique features of glycolytic pathways in Archaea. Biochem. J. *375*, 231–246.

Wallace, A.C., Laskowski, R.A., and Thornton, J.M. (1995). LIGPLOT: a program to generate schematic diagrams of protein ligand interactions. Protein Eng. *8*, 127–134.

Wright, S.W., Carlo, A.A., Carty, M.D., Danley, D.E., Hageman, D.L., Karam, G.A., Levy, C.B., Mansour, M.N., Mathiowetz, A.M., McClure, L.D., et al. (2002). Anilinoquinazoline inhibitors of fructose 1,6-bisphosphatase bind at a novel allosteric site: synthesis, in vitro characterization, and X-ray crystallography. J. Med. Chem. *45*, 3865–3877.

Zhang, R., Villeret, V., Lipscomb, W.N., and Fromm, H.J. (1996). Kinetics and mechanisms of activation and inhibition of porcine liver fructose-1,6-bisphosphatase by monovalent cations. Biochemistry *35*, 3038–3043.

Accession Numbers

The coordinates and structure factors have been deposited in the Protein Data Bank (accession code 1UMG).